Research Article

A thermal method for obtention of 2 to 3 reduced graphene oxide layers from graphene oxide

J. C. Silva Filho[1] · E. C. Venancio[1] · S. C. Silva[2] · H. Takiishi[2] · L. G. Martinez[2] · R. A. Antunes[1]

Received: 16 March 2020 / Accepted: 21 July 2020 / Published online: 29 July 2020
© Springer Nature Switzerland AG 2020

Abstract
In this work, a thermal reduction method was developed to obtain reduced graphene oxide (rGO) with 2 or 3 layers from graphene oxide (GO). The GO X-ray diffraction (XRD) patterns presented diffraction peak at 2θ = 10°, which is related to (002) reflection. After heat treatment under nitrogen (N_2(g)) atmosphere, this peak was shifted to 2θ = 25°, presenting an interlayer distance of 3.8 Å, associated to GO reduction. BET analysis of modified GO samples identified an average pore diameter of 45.38 Å and surface area of 23.06 m^2/g. In the case of rGO_1, rGO_2 and rGO_3 samples, they presented surface areas from 32.47 to 612.74 m^2/g and an average pore diameter of 108.21–149.54 m^2/g. Thermogravimetric analysis (TGA) indicated a higher mass loss between 150 and 230 °C. Raman spectra showed ID/IG ratios of rGO samples were higher than GO (1.36-GO; 1.45-rGO_1, 1.87-rGO_3) due to reducing GO and increasing sp^2 clusters. XPS analysis revealed that the main carbon species in the samples were sp^2-type bonds (14.99 at% for the GO and 47.85 at% for rGO_3). The FTIR spectra of rGO_1, rGO_2 and rGO_3 samples presented peaks at 3454.22 cm^{-1} (hydroxyl) and 1077.43 cm^{-1} (C–O).

Keywords Reduced graphene oxide · Graphene oxide · Thermal treatment · Few layers graphene

1 Introduction

Carbon has a large number of allotropes and its properties are related to the hybridization state of the carbon atoms [1]. The chemical exfoliation of graphite has been considered as a strategy capable of producing graphene oxide (GO) [2]. Initially, the oxidation of graphite is promoted by introducing functional groups, such as hydroxyl and epoxide groups, which decrease the interactions between the layers. As a consequence, the spacing between them increases. A greater space between the layers facilitates the exfoliation of graphite oxide in simple sheets [3]. The synthesis of graphene from the reduction of graphene oxide allows the control of properties, such as electrical and thermal conduction, surface area and dispersibility in different solvents [4]. One method that has been used in the thermal reduction of GO is carried out in the presence of different gases and temperature conditions [5]. Among all the methods developed so far, thermal reduction of GO may be one of the most promising routes to obtain reduced graphene oxide (rGO) and graphene in large quantities [6]. Heating of GO in inert gas is called thermal reduction because the main objective is to produce a solid obtained from the carbon atoms transformed into reduced and oxidized forms that are mainly by-products of the gaseous phase of carbon oxide, such as CO and CO_2 [7]. Owing to hydrophilic properties, associated with the presence of functional groups containing oxygen on its surface, GO and rGO can be, potentially, highly reactive to changes occurring in the surface of functional groups, during the reduction process [3]. The physical properties of graphene can be very sensitive to the number of layers. Therefore, in general, the number of layers and the crystallite size are fundamental to the understanding of these

✉ J. C. Silva Filho, jorgecsilvaf@gmail.com | [1]Federal University of ABC, Santo André, Brazil. [2]Materials Science and Technology Centre, Nuclear and Energy Research Institute, São Paulo, Brazil.

SN Applied Sciences (2020) 2:1450 | https://doi.org/10.1007/s42452-020-03241-9

properties [8]. In this work, GO was synthesized using the modified Hummers' method. The heat treatment for GO reduction to rGO was performed under inert nitrogen gas (N_2(g)) atmosphere and partial pressure of 10 kPa, varying the time, heating rate and temperature of the process. The aim was to produce reduced graphene oxide with less than four layers and to control its surface area.

2 Experimental details

2.1 Preparation of GO

Graphene oxide was synthesized from graphite powder (*Nacional de Grafite*, at 99.99% purity) by using the modified Hummers' method. Graphite was added into a flask containing sulfuric acid (H_2SO_4), potassium permanganate ($KMnO_4$) and phosphoric acid (H_3PO_3). The mixture was kept under vigorous stirring, and then hydrogen peroxide (H_2O_2) was added. Thereafter, the mixture was centrifuged, washed with hydrochloric acid (HCl), subsequently washed and exfoliated by using methoxyethane.

2.1.1 Preparation for GO heat treatment

The heat treatments for obtaining the reduced graphene oxide samples are shown in Fig. 1. Three different routes were employed. The samples were designated as rGO_1, rGO_2 and rGO_3, as indicated in Fig. 1. The samples were obtained using different temperature steps, times and heating rates. The choice of these processing routes was based on previous trials in our laboratory, aiming at increasing the mass of rGO obtained at the end of the thermal reduction process, eliminating micro-explosions and avoiding expansion of the rGO surface area.

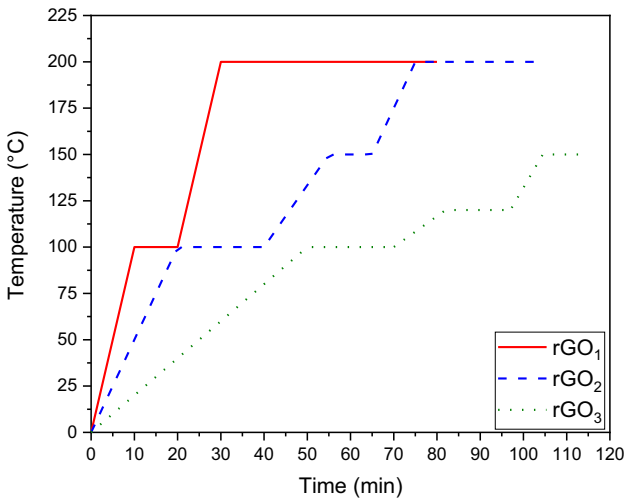

Fig. 1 Heat treatment procedures for obtaining the rGO samples

2.2 Characterization of GO and rGO

Thermogravimetric analyses (TGA) were carried out by using TA Universal V4.5A instrument. Samples (3 mg) were subject to heating at 20 °C/min, from room temperature up to 800 °C under nitrogen gas atmosphere. Fourier transform infrared spectroscopy (FTIR) spectra were recorded by a Nexus 870 spectrometer (Thermo Nicolet). X-ray photoelectron spectroscopy (XPS) was employed to analyze the surface chemical states of the different samples. The spectra were obtained by using a ThermoFisher Scientific K-alpha + spectrometer operating with Al-kα (1486.6 eV) radiation source. The pressure in the analysis chamber was approximately 10^{-7} Pa. The spot size was 400 µm. The spectra were fitted using a combination of Lorentzian-Gaussian curves in the CASA software. The Shirley algorithm was employed for background subtraction. Raman spectra were recorded in the range of 500–2000 cm^{-1} using a Raman WITEC instrument (Confman Raman Alpha 300r-green laser microscope, 532 nm; 45 mW). X-ray diffraction (XRD) experiments were carried out by using a Bruker D8 Advantage instrument with a copper tube, at 40 kV and 30 mA. XRD showed the interplanar spacing of the samples that can be determined by Bragg's Law and the crystallite size of was obtained by using Scherrer's equation. Brunauer, Emmelt and Teller (BET) surface and pore analyses were carried out by using adsorption analyzer equipment, model ASAP 2010 (Micromeritics).

3 Results and Discussion

TGA measurements were performed to assess the thermal stability of GO and rGO samples. Figure 2a shows the TGA curve for GO. It indicates that its mass loss takes place in two stages. About 12% mass loss occurred below 120 °C primarily due to the loss of water molecules adsorbed in GO [9]. In the second stage, roughly 2.55% of mass loss takes place at ~ 280 °C due to thermal decomposition of oxygen-containing functional groups of carboxyl, hydroxyl and epoxy groups in the edge and basal planes. Similar results were reported in the literature [10, 11]. The mass loss becomes faster as temperature is raised. The residual mass at the end of the experiment was approximately 50%.

Figure 2b–d are related to samples rGO_1, rGO_2 and rGO_3. Comparing the TGA curve of GO in Fig. 2a with rGOs in Fig. 2b–d, it is evident that GO decomposes in different stages. The mass losses of 5% (rGO_1, rGO_2) and 8% (rGO_3) at 120 °C were attributed to decomposition of residual

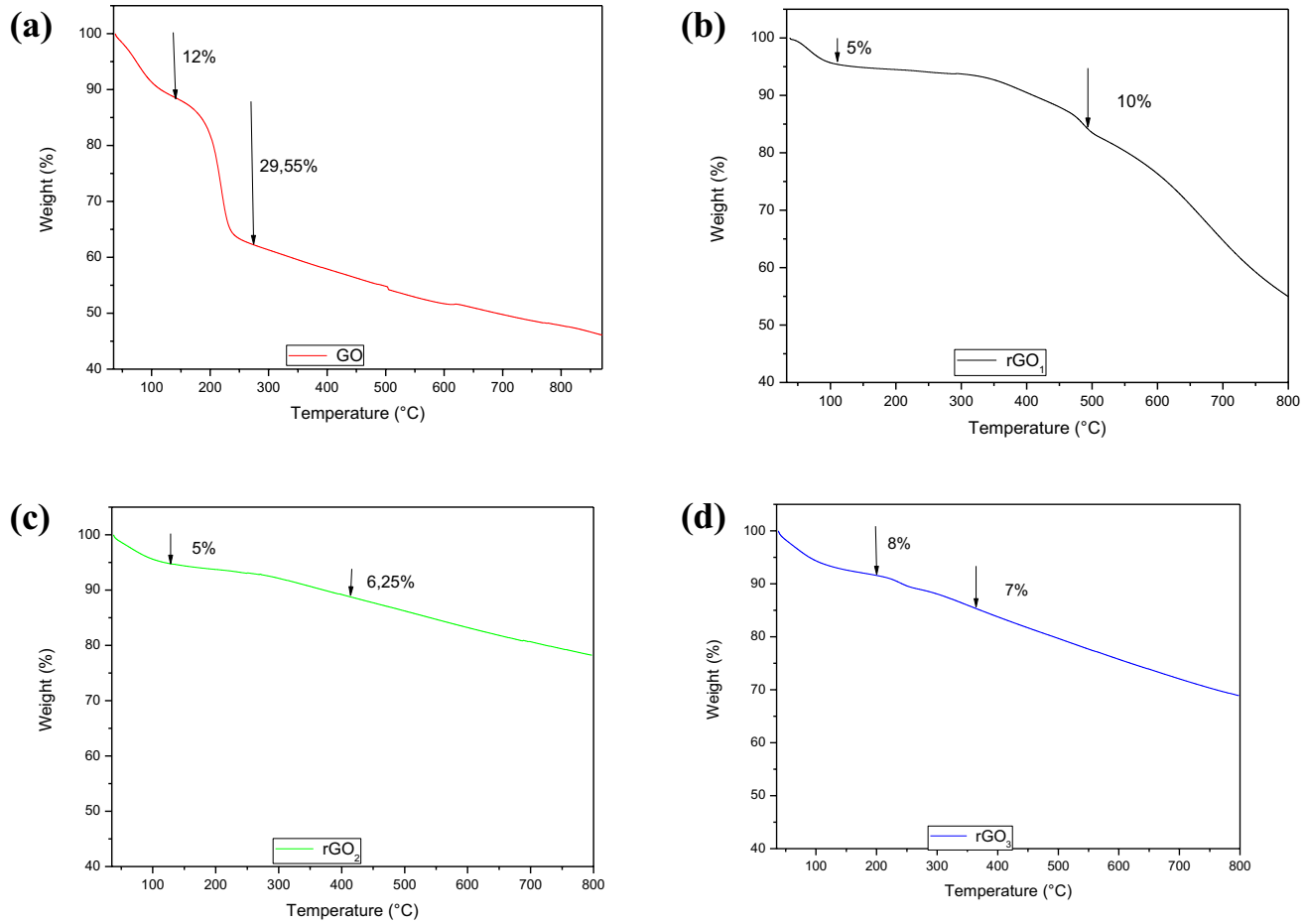

Fig. 2 TGA curves for **a** GO and for different rGO samples, **b** rGO_1, **c** rGO_2, and **d** rGO_3

water and volatiles [12]. Figure 2b (rGO_1) corresponds to the heat treatment carried out at a higher temperature and longer time, when compared with the other samples (rGO_2 and rGO_3). Throughout the TGA analysis the mass gradually decreased in the case of rGO_2 and rGO_3, and decreased markedly for rGO_1, showing a higher mass loss rate. This can be explained by the micro-explosions resulting from the highly exothermic reaction that occur at the end of the heat treatment for rGO_1, due to the treatment conditions and residual impurities of GO synthesis [13].

In Fig. 3, BET results show the changes in the relative pressure and absorbed quantity of N_2 for the different samples. From these analyses, GO presented an average pore diameter of 45.38 Å and surface area of 23.06 m^2/g. Controlling the variables of the thermal reduction achieved surface area of 32.47 m^2/g in rGO_1 and rGO_3 samples with an average pore diameter of 108.21 Å. While sample rGO_2—that presented surface area expansion—has surface area 612.74 m^2/g and average pore diameter 149.54 Å.

Distinction between the explosive and non-explosive character of the thermal reduction process depends on its experimental parameters. Therefore, the temperature, heating rate and step employed in the thermal processing of rGO_1, resulted in an explosive process which could be

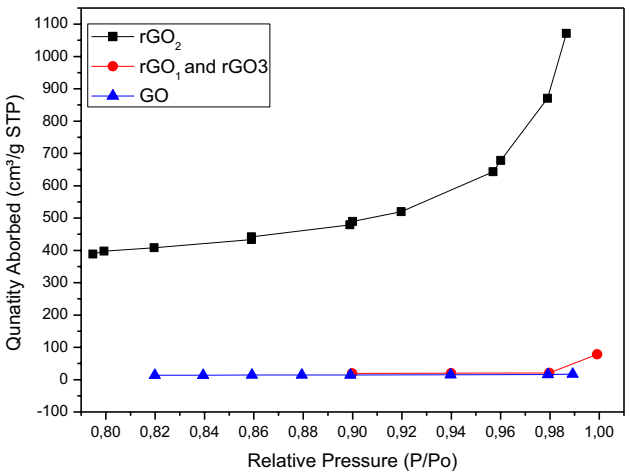

Fig. 3 BET curves for **a** GO and rGOs

avoided when decreasing heating rate and temperatures were employed such as in the production of rGO_2 and rGO_3. However, when the heating rate is still high (rGO_2 sample), it results in surface area expansion. In the rGO_3 sample, the heating rate and reduction of the treatment time enabled process control and avoided the occurrence of explosion (rGO_1) and surface area expansion (rGO_2). Explosive reduction leads to higher surface areas, as fracture causes early gas release that limits internal pressure development [13]. These different surface areas and average pore diameters are closely related to the structure and number of layers of the graphene oxide species, as also observed in the literature [14].

Figure 4 presents the FTIR spectra of GO and rGOs. The peak at 3452.22 cm^{-1} is related to OH [15]. Peaks at 2362.76 cm^{-1} may be assigned to the axial atmospheric CO_2 vibrations [16]. Other peaks were found at 1715.51 cm^{-1} which can be assigned to carbonyl groups ((C=O from carboxylic acids or ketones) [15]; 1619.62 cm^{-1} (C=C), which normally has low intensity because it is related to conjugated alkenes [17]; 1381.33 cm^{-1} (CH_3), angular deformation; 1077.43 cm^{-1} (C–O), alcohol [12].

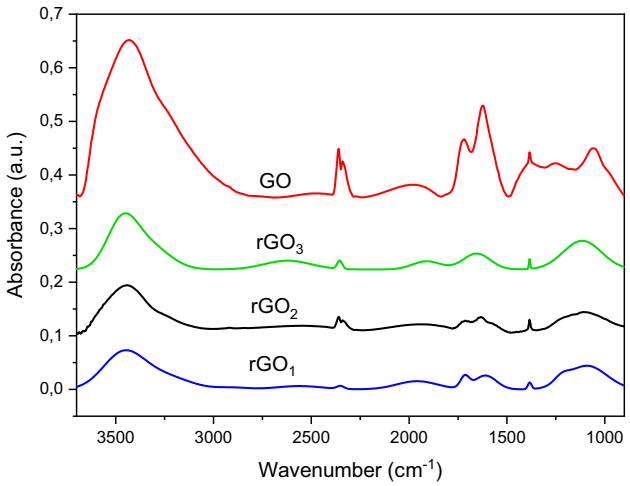

Fig. 4 FTIR spectra of GO and rGOs

Characteristic XPS spectra for the GO and rGO samples in the C1s and O1s regions are presented in Figs. 5 and 6, respectively. The main chemical species and their atomic concentrations are summarized in Tables 1 and 2. Figure 5 shows four peaks in the C1s region: carbon sp^2, at 284.70 eV (14.99 at%), C–OH, at 286.60 eV (48.07 at%), C–O–C, at 287.88 eV (26.88 at%) and $\pi - \pi^*$, at 290.70 eV (10.06 at%) [18–20]. The O 1 s region of the GO sample presented three different components at 532.18 eV (18.35 at%), 534.60 eV (76.62 at%), 535.70 eV (5.03 at%), which are related to C=O, C–O–C and H_2O groups [5, 21], respectively.

Figure 6 shows the XPS spectra in the C1s (a) and (b) O1s regions of rGO_1, rGO_2 and rGO_3. When the heat treatment was performed at 2 °C/min with three temperature steps (route for obtaining rGO_3) the C1s region presented only two different components whereas three types of carbon bonds were found in the C1s region of the pristine graphene oxide (GO). Also, an increase in atomic percentage of the sp^2 carbon bonds was observed for the three rGO samples. Table 1 shows the heat treatment was effective at increasing the quantity of carbon–carbon double bonds. Initially, GO sample had 14.99 at% and, after heat treatment, rGO_1, rGO_2 and rGO_3 samples had 35.51 at%, 33.14 at% and 47.85 at% sp^2. Another factor was the reduction of hydroxyl groups (Table 2-O1s regions) in the rGOs, rGO_2 (23.91 at%) e rGO_3 (12.90 at%), when compared to GO (48.07 at%). For the rGO_1 e rGO_3 samples, it was not possible to eliminate adsorbed H_2O from the surface, showing that a high heating rate does not promote water removal during the heat treatment.

Figure 7 shows the Raman spectra obtained for GO and rGO samples. The positions of D, G and 2D bands are indicated in the figure as well as the ID/IG ratios. Two

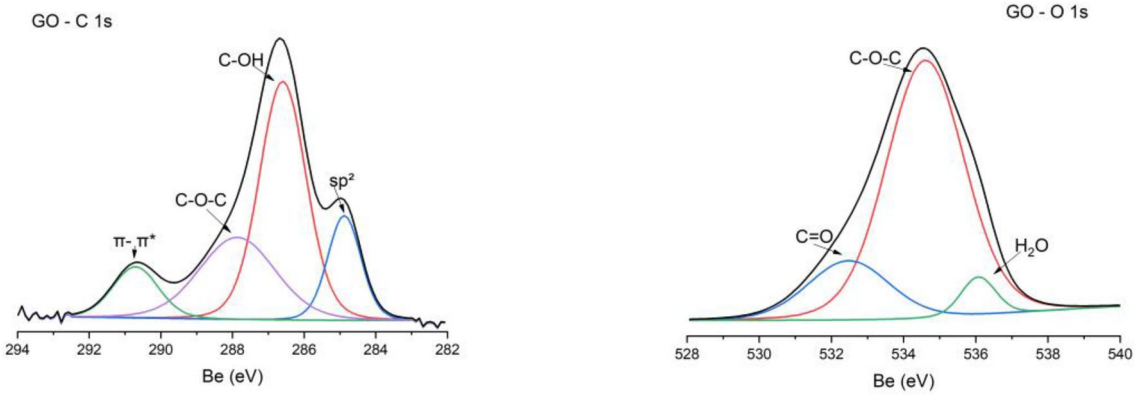

Fig. 5 XPS spectra in the C1s **a** and **b** O1s regions of GO

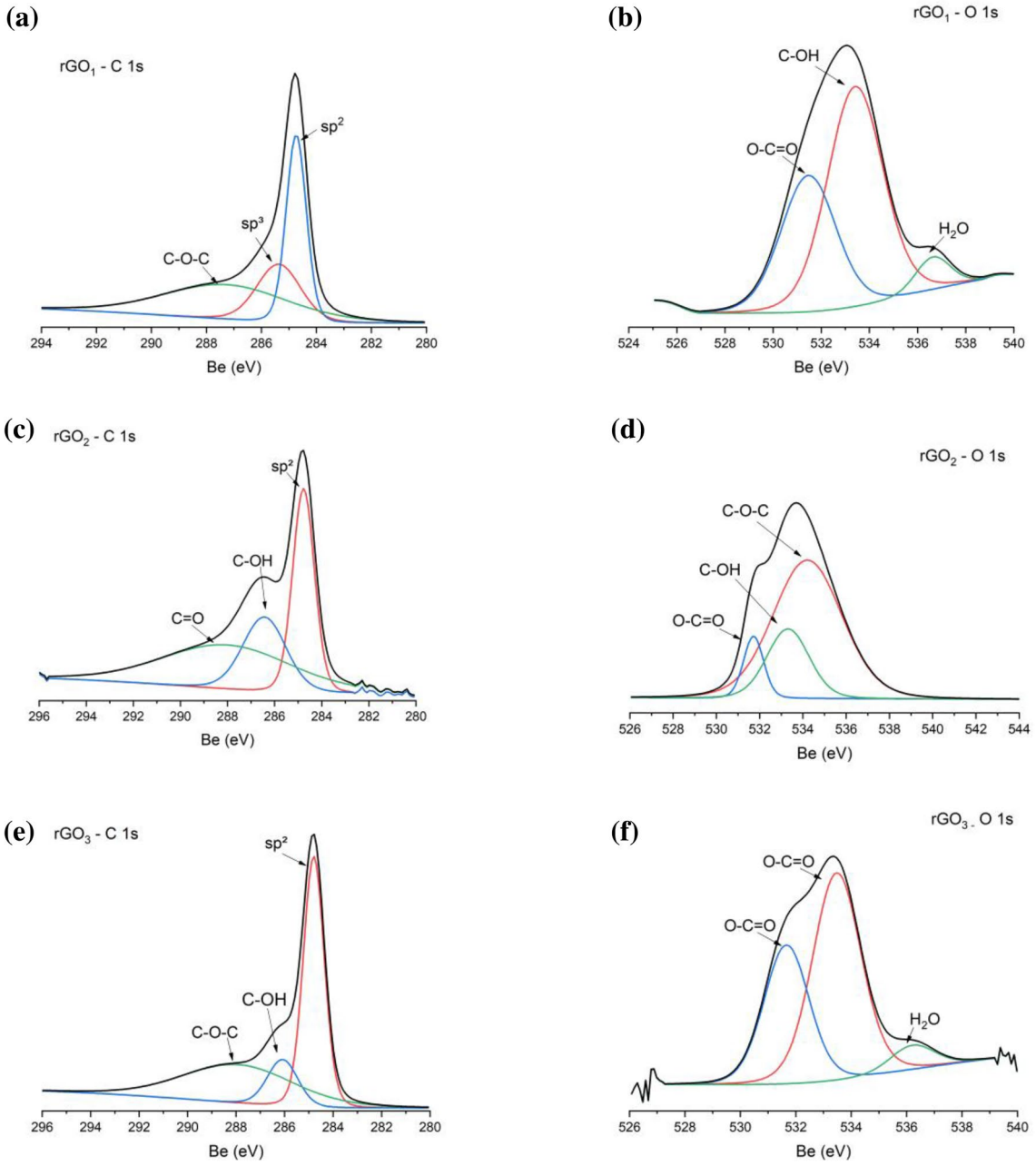

Fig. 6 XPS spectra in the C1s (**a**, **c**, **e**) and (**b**, **d**, **f**) O1s regions of rGO_1, rGO_2 and rGO_3

Table 1 Fitting results for the C1s region of GO and rGOs

Sample	Component (at.%)					
	C sp^2	C sp^3	C–OH	C–O–C	C=O	$\pi-\pi^*$
GO	14.99	–	48.07	26.88	–	10.06
rGO_1	35.51	33.68	–	40.81	–	–
rGO_2	33.14	–	23.91	–	42.95	–
rGO_3	47.85	–	12.90	39.25	–	–

Table 2 Fitting results for the O1s region of GO and rGOs

Sample	Component (at.%)				
	O–C=O	C=O	C–OH	C–O–C	H_2O
GO	–	18.35	–	76.62	5.03
rGO_1	35.93	–	58.56	–	5.50
rGO_2	9.07	–	21.41	69.52	–
rGO_3	36.112	–	57.72	–	6.15

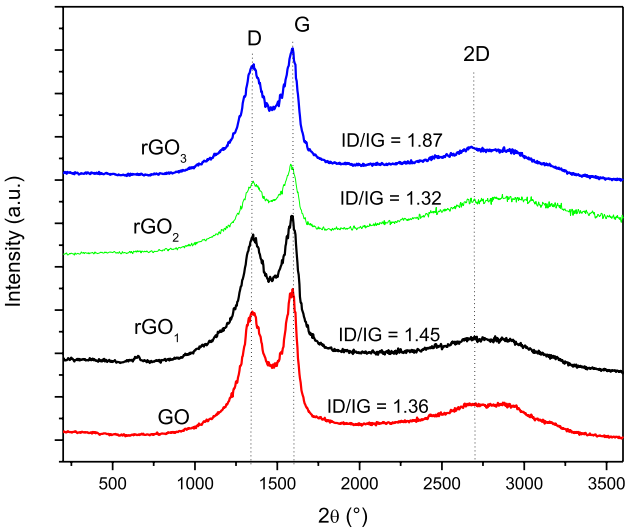

Fig. 7 Raman spectra of GO and rGOs

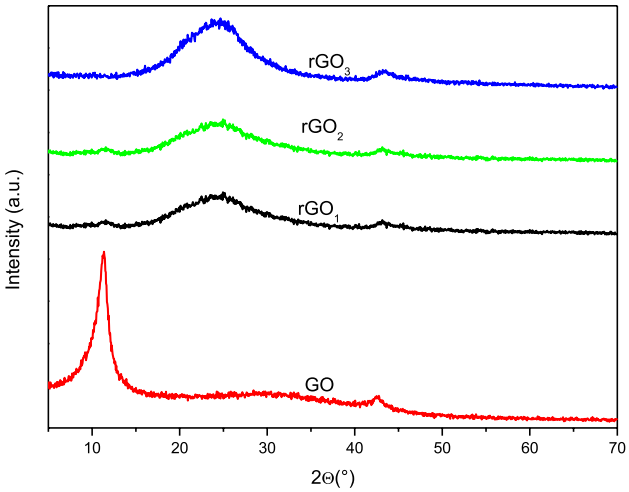

Fig. 8 XRD patterns of GO and rGOs

Table 3 Crystal size and interatomic distance of GO and rGOs

Samples	*d* middle (Å)	Crystallite size (nm)	Crystalline layers
GO	7.9	56.7	7.2
rGO_1	3.7	10.7	2.9
rGO_2	3.7	10.8	2.9
rGO_3	3.8	9.2	2.4

bands are seen, one at 1579.42 cm^{-1} related to sp^2 carbon atoms (G band) and the second one at 1364.57 cm^{-1} (D band) which is attributed to defects related to sp^3 carbons, located in the sp^2 carbon crystal lattice. A verybroad band at 2685.62 cm^{-1} is also observed, the 2D band, which is related to graphene structure defects [22, 23]. After the heat treatments, D, G and 2D bands are shifted in rGO_1 (1360.06 cm^{-1}, 1576.85 cm^{-1}, 2716.39 cm^{-1}), rGO_2 (1359.21 cm^{-1}, 1580.81 cm^{-1}, 2673.23 cm^{-1}) and rGO_3 (1347.59 cm^{-1}, 1593.05 cm^{-1}, 2725.13 cm^{-1}) samples. The higher intensity of D bands with respect concerning G bands indicates an increase in the amount of disordered phase in rGOs. The present oxygen atoms cause increase in the interplanar distance and change the materials structures vibrations. The ID/IG ratio is a measure of the disorder degree and is inversely proportional to the average cluster size sp^2 [24]. Figure 7 shows the ID/IG ratios of rGOs were higher than that of GO (1.36), revealing an increasing trend for rGO1 (1.45) and rGO3 (1.87). This suggests that new or more graphitic domains are formed and the sp^2 cluster number is increased [25, 26]. This information was also observed from the XPS fitting results shown in Table 1 as the content of sp^2 bonds increased from 14.99% for GO to 47.88% for rGO_3.

Figure 8 shows XRD patterns for GO and rGOs. Using Bragg's Law and Sherrer's equation ($k = 0{,}9$ Å) the values of interplanar spacing, crystallite size and number of crystalline layers were obtained, as displayed in Table 3. The peak centered at $2\theta \approx 12°$ corresponds to the (002) crystalline plane. After heat treatment and thermal reduction, the peak was shifted to $2\theta \approx 24°$. Since this peak corresponds to the layer-to-layer distance (*d*) [27], shifting X-ray peaks of rGOs to a higher angle results in decreasing *d*-spacing, showing that the thermal reduction process decreases the interplanar spacing. These results indicate a separation of the layers and oxygen removal during the thermal reduction process, i.e., TGA and XRD results demonstrated that the GO synthesis was successfully performed with the reduction of samples rGO_1, rGO_2 and rGO_3. When these results are compared to the literature, it is possible to observe that different temperatures are used for the thermal reduction treatment, i.e., from 500 to 1000 °C [28–30], and heating rates between 10 and 80 °C/s. These works show narrower interlayer spacing, i.e., 4 Å [28, 31]. However, in our work the reduction of graphene oxide

was carried out at a maximum temperature of 200 °C, which resulted in the change of the characteristic GO XRD reduction peak, reducing crystallite size and maintaining the number of layers between 2 and 3, regardless of the parameters used in the thermal reduction route.

In Table 3, the distances between the electronic layers, the crystallite size and number of crystalline layers are shown. For GO, the interplanar distance was 7.9 Å and for the samples subjected to heat treatment (rGO_1, rGO_2 and rGO_3), these distances were between 3.7 and 3.8 Å. The decrease in crystallite size may also be observed from 56.7 nm for GO sample to 10.7 nm, 10.8 nm and 9.2 nm for rGO_1, rGO_2 and rGO_3, respectively. The number of crystalline layers of rGOs was also decreased with respect to concerning GO. The results show that reduced graphene oxide produced by thermal exfoliation at high temperature exhibits a few-layered structure. Hence, it has higher specific surface area. Similar results were obtained by other authors for thermally reduced graphene oxide samples [32, 33].

4 Conclusions

The heat treatment method developed in this work was efficient at reducing 7 GO layers to 2 to 3 rGO layers, as observed by XRD. The thermal reduction process made it possible to change the crystallite size, distance between layers, number of crystalline layers, surface area and chemical composition. It was shown for the first time that the rGO thermal reduction was carried out without explosion and with a decrease in the total number of rGO layers, from 8 GO layers to 3 rGO layers at the end of the thermal reduction process. Raman and XPS spectra confirm the increase in the number of carbon sp^2 bonds at different thermal reduction routes. BET analysis confirms the possibility of controlling the expansion of rGOs depending on the process parameters such as heating rate, temperature step and treatment time.

Acknowledgements INCT Project: CNPQ (465719/2014-7), FAPESP (2014/50887-4) and CAPES (23038000776/2017-54), the Materials Science and Technology Center (CCTM/IPEN), Nuclear Fuel Center (CCN/IPEN), Laboratory of Electrical Engineering (POLI/USP), the Multiuser Laboratory of Functional Polymers (UFABC), the National Graphite and IPEN-CNEN/SP for the infrastructure.

Funding This study was funded by INCT Project: CNPQ (465719/2014-7), FAPESP (2014/50887-4) and CAPES (23038000776/2017-54).

Compliance with ethical standards

Conflict of interest The authors declare that they have no conflict of interest.

References

1. Yan P, Zhang B, Su W, Qi DW (2019) Surface chemistry of nanocarbon: characterization strategies from the viewpoint of catalysis and energy conversion. Carbon 143:915–936. https://doi.org/10.1016/j.carbon.2018.11.085
2. Stankovich S, Piner RD, Nguyen ST, Ruoff RS (2006) Synthesis and exfoliation of isocyanate-treated graphene oxide nanoplatelets. Carbon 44:3342–3347. https://doi.org/10.1016/j.carbon.2006.06.004
3. Sengupta I, Chakraborty S, Talukdar M, Pal SK, Chakraborty S (2018) Thermal reduction of graphene oxide: how temperature influences purity. J Mater Res 33:4113–4122. https://doi.org/10.1557/jmr.2018.338
4. Toh SY, Loh KS, Kamarudin SK, Daud WRW (2014) Graphene production via electrochemical reduction of graphene oxide: synthesis and characterisation. Chem Eng J 251:422–434. https://doi.org/10.1016/j.cej.2014.04.004
5. Drewniak S, Muzyka R, Stolarczyk A, Pustelny T, Kotyczka-Morańska M, Setkiewicz M (2016) Studies of reduced graphene oxide and graphite oxide in the aspect of their possible application in gas sensors. Sensors 16:103. https://doi.org/10.3390/s16010103
6. Chen Y, Egan GC, Wan J, Zhu S, Jacob RJ, Zhou W, Fu K (2016) Ultra-fast self-assembly and stabilization of reactive nanoparticles in reduced graphene oxide films. Nat Commun 7:12332. https://doi.org/10.1038/ncomms12332
7. Gao X, Jang J, Nagase S (2009) Hydrazine and thermal reduction of graphene oxide: reaction mechanisms, product structures, and reaction design. J Phys Chem C 114:832–842. https://doi.org/10.1021/jp909284g
8. Kauling AP, Seefeldt AT, PisoniDP PR, Bentini R, Oliveira RV, Castro Neto AH (2018) The Worldwide graphene flake production. Adv Mater 30:1803784. https://doi.org/10.1002/adma.201803784
9. Gao R, Hu N, Yang Z, Zhu Q, Chai J, Su Y, Zhang Y (2013) Like graphene-Ag composite films with enhanced mechanical and electrical properties. Nanoscale Res Lett 8:32. https://doi.org/10.1186/1556-276X-8-32
10. Rajagopalan B, Chung JS (2014) Reduced chemically modified graphene oxide for supercapacitor electrode. Nanoscale Res Lett 9:535. https://doi.org/10.1186/1556-276X-9-535
11. Ossonon BD, Bélanger D (2017) Synthesis and characterization of sulfophenyl-functionalized reduced graphene oxide sheets. RSC Adv 7:27224–27234. https://doi.org/10.1039/C6RA28311J
12. Silva Filho JC, Soares E, Venancio E, Silva S, Takiishi (2017) Influência do tratamento térmico na redução do óxido de grafeno. ISSN 2358-2359, Doi: 10.5151/phypro-viii-efa-18
13. Qiu Y, Guo F, Hurt R, Külaots I (2014) Explosive thermal reduction of graphene oxide-based materials: mechanism and safety implications. Carbon 72:215–223. https://doi.org/10.1016/j.carbon.2014.02.005
14. Dai JF, Wang GJ, Ma L, Wu CK (2015) Surface properties of graphene: relationship to graphene-polymer composites. Rev Adv Mater Sci 40:60–71
15. Si Y, Aamulski ETS (2008) Synthesis of water soluble graphene. Nano Lett 8:1679–1682. https://doi.org/10.1021/nl080604h
16. Priante F, Salim M, Ottaviano L, Perrozzi F (2018) XPS study of graphene oxide reduction induced by (100) and (111)-oriented Si substrates. Nanotechnology 29:075704
17. Yang B, Liu Z, Guo Z, Zhang W, Wan M, Qi X, Zhong H (2014) In situ green synthesis of silver–graphene oxide nanocomposites by using tryptophan as a reducing and stabilizing agent and their application in SERS. Appl Surf Sci 316:22–27. https://doi.org/10.1016/j.apsusc.2014.07.084

18. Wi G (2015) The chemistry of graphene oxide. Graphene oxide. Springer 39:61–95. https://doi.org/10.1039/B917103G
19. Shim S, Kim KT, Lee J, Jo W (2012) Facile method to functionalize graphene oxide and its application to poly (ethylene terephthalate)/graphene composite. ACS Appl Mater Interfaces 4:4184–4191. https://doi.org/10.1021/am300906z
20. Jovanovic SP, Markovi ZM, Svrgiannis Z, Dramicanin MD, Arcudi F, Pv PV, Markovi BMT (2017) Enhancing photoluminescence of graphene quantum dots by thermal annealing of the graphite precursor. Mater Res Bull 93:183–193. https://doi.org/10.1016/j.materresbull.2017.04.052
21. Bagri A, Mattevi C, Acik M, Chabal YJ, Cchhowalla M, Shenoy VB (2010) Structural evolution during the reduction of chemically derived graphene oxide. Nat Chem 2:581. https://doi.org/10.1038/nchem.686
22. Ferrari AC, Meyer JC, Scardaci V, Casiraghi C, Lazzeri M, Mauri F, Geim AK (2006) Raman spectrum of graphene and graphene layers. Phys Rev Lett 97:187401. https://doi.org/10.1103/PhysRevLett.97.187401
23. Wu JB, Lin ML, Cong X, Liu HN, Tan PH (2018) Raman spectroscopy of graphene-based materials and its applications in related devices. Chem Soc Rev 47:1822–1873. https://doi.org/10.1039/C6CS00915H
24. Perez LA, Bajales N, Lacconi GI (2019) Raman spectroscopy coupled with AFM scan head: a versatile combination for tailoring graphene oxide/reduced graphene oxide hybrid materials. Appl Surf Sci. https://doi.org/10.1016/j.apsusc.2019.143539
25. Guoa Y, Suna X, Liua Y, Wangb W, Qiua H, Gao J (2012) One pot preparation of reduced graphene oxide (RGO) or Au (Ag) nanoparticle-RGO hybrids using chitosan as a reducing and stabilizing agent and their use in methanol electrooxidation. Carbon 50:2513–2523. https://doi.org/10.1016/j.carbon.2012.01.074
26. Wang S, Dong Y, He C, Gao Y, Jia N, Chen Z, Song W (2017) The role of sp_2/sp_3 hybrid carbon regulation in the nonlinear optical properties of graphene oxide materials. RSC Advances 78:53643–53652. https://doi.org/10.1039/C7RA10505C
27. Cullity BD (1956) Elements of X-ray diffraction. Add Ison-Wesley Publishing Company Inc, Oxford
28. Yang H, Kannappan S, Pandian AS, Jang JH, Lee YS, Lu W (2017) Rapidly annealed nanoporous graphene materials for electrochemical energy storage. J Mater Chem A 5:23720–23726. https://doi.org/10.1039/C7TA07733E
29. De Silva KKH, Huang HH, Joshi R, Yoshimura M (2020) Restoration of the graphitic structure by defect repair during the thermal reduction of graphene oxide. Carbon 166:74–90. https://doi.org/10.1016/j.carbon.2020.05.015
30. Ambrosi A, Chua CK, Bonanni A, Pumera M (2014) Electrochemistry of graphene and related materials. Chem Rev 114:7150–7188. https://doi.org/10.1021/cr500023c
31. Zhou Y, Lin X, Huang Y, Guo Y, Gao C, Xie G, Jiang Y (2016) Impact of further thermal reduction on few-layer reduced graphene oxide film and its np transition for gas sensing. Sens Actuators B Chem 235:241–250. https://doi.org/10.1016/j.snb.2016.05.078
32. Wypych G (2019) Graphene important results and applications. Mater Performance Character. https://doi.org/10.1016/B978-1-927885-51-2.50005-5
33. Sekimoto Y, Ohtani R, Nakamura M, Koinuma M, Lindoy LF, Hayami S (2017) Tuneable pressure effects in graphene oxide layers. Sci Rep 7:12159. https://doi.org/10.1038/s41598-017-12444-x

Publisher's Note Springer Nature remains neutral with regard to jurisdictional claims in published maps and institutional affiliations.